Supporting Information

A Novel 2D Carbon material T-graphene supported 3d Transition Metals as Efficient

Oxygen Reduction Catalysts

Run Jiang, Zelong Qiao, Haoxiang Xu, Dapeng Cao*

State Key Laboratory of Organic-Inorganic Composites, Beijing University of Chemical

Technology, Beijing 100029, People's Republic of China

*Email: caodp@mail.buct.edu.cn

1 Computation Details

1.1 DFT computational methods

All calculations were based on the first principles under the framework of spin-polarized density functional theory (DFT), using the Vienna ab initio simulation package (VASP) code[1, 2], and using the Perdew-Burke-Ernzerhof (PBE) functional[3-6] to model the exchange correlation energy under the generalized gradient approximation (GGA). The projection enhanced wave (PAW) pseudopotential[7] was used to describe ionic nuclei. The plane-wave cut-off energy of 500 eV was adopted. The convergence threshold of iteration in self-consistent field (SCF) was set to 10^{-5} eV per atom for energy and 0.02 eV Å^{-1} for the force. The Gauss smearing of 0.05 eV was used for orbital occupation. Moreover, to solve the non-localization problem that the PBE exchange correlation function cannot accurately describe the electronic interaction of transition metal atoms, the DFT+U method[8-12] was applied through the rotation invariant method, and the value of U−J of the 3d-orbitals of 3d transition metals are set as shown in **Table S1**. A Γ-centered Monkhorst-Pack 3×3×1 k-point grid was used to sample the Brillouin zone for structural optimization. A large

vacuum plate of 20 Å in the z direction was insert for surface isolation to prevent the interaction between two adjacent surfaces. DFT-D3 method with Becke-Jonson damping[13, 14] was used for vdW corrections. VASP-sol package[15] was used to simulate the solution environment, where the dielectric constant was set to 80. The Lobster software[16] was used to perform the COHP analysis[17], and obtain the bonding and anti-bonding information. VASP-kit code[18] was used to extract electronic density of states.

1.2 ORR reaction free energies

The ORR pathway on SACs were calculated in detail according to electrochemical framework developed by Nørskov and his co-workers[19, 20]. For each elementary step, the Gibbs reaction free energy ΔG is defined as the difference between free energies of the initial and final states and is given by the expression:

$$\Delta G = \Delta E + \Delta ZPE - T\Delta S + \Delta G_U + \Delta G_{pH} \tag{1}$$

where ΔG_U is the free energy change caused by the applied potential U ($\Delta G_U = -neU$), and U is the applied potential vs. RHE electrode, e is the transferred elementary charge and n is the transferred proton-electron pairs. ΔG_{pH} is the corrected value of H^+ free energy ($\Delta G_{pH} = -k_BT \ln[H^+] = pH \times k_BT \ln10$, where k_B is the Boltzmann constant and T is the temperature). According to Nernst equation, $U^0_{RHE} = 1.23$ V.

Therefore, the reaction free energy of ΔG_1, ΔG_2, ΔG_3, ΔG_4 for ORR can be calculated using the following equations:

$$\Delta G_1 = \Delta G_{*OOH} - 4.92 + \Delta G_U + \Delta G_{pH} \tag{2}$$

$$\Delta G_2 = \Delta G_{*O} - \Delta G_{*OOH} + \Delta G_U + \Delta G_{pH} \tag{3}$$

$$\Delta G_3 = \Delta G_{*OH} - \Delta G_{*O} + \Delta G_U + \Delta G_{pH} \tag{4}$$

$$\Delta G_4 = -\Delta G_{*OH} + \Delta G_U + \Delta G_{pH} \tag{5}$$

Since it is difficult to obtain the exact free energy of O, OH and OOH radicals in the electrolyte solution, the adsorption free energy ΔG_{*O}, ΔG_{*OH}, and ΔG_{*OOH} are relative to the free energy of stoichiometrically appropriate amounts of H_2O and H_2, defined as follows:

$$\Delta G_{*O} = E_{*O} + E_{H_2} - E_{H_2O} - E* + \Delta ZPE - T\Delta S \tag{6}$$

$$\Delta G_{*OH} = E_{*OH} + 0.5 \times E_{H_2} - E_{H_2O} - E* + \Delta ZPE - T\Delta S \tag{7}$$

$$\Delta G_{*OOH} = E_{*OOH} + 1.5 \times E_{H_2} - 2 \times E_{H_2O} - E* + \Delta ZPE - T\Delta S \tag{8}$$

where ΔE is the reaction energy of reactants and product adsorbed on the catalyst surface; ΔZPE and ΔS are the zero-point energy and entropy correction.[1] The values used for zero-point energy corrections of intermediates are listed in **Table S2**. Energy values for H_2O, O_2 and H_2 are listed in **Table S3**.

1.3 bond order

The bond order is defined as half the difference between the number of bonding electrons and the number of anti-bonding electrons[21]:
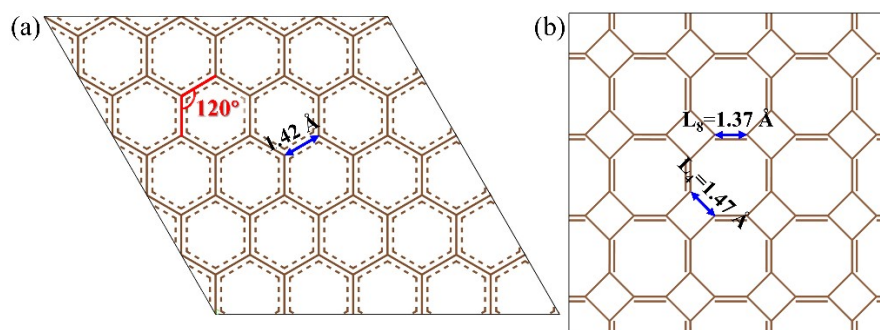
$$\text{bond order} = (N_{bonding} - N_{anti-bonding}) / 2 \tag{9}$$

where $N_{bonding}$ and $N_{anti-bonding}$ represent the electrons number of bonding and anti-bonding, respectively. The higher the bond order, the stronger the orbital interaction between cations and oxygenated intermediates.
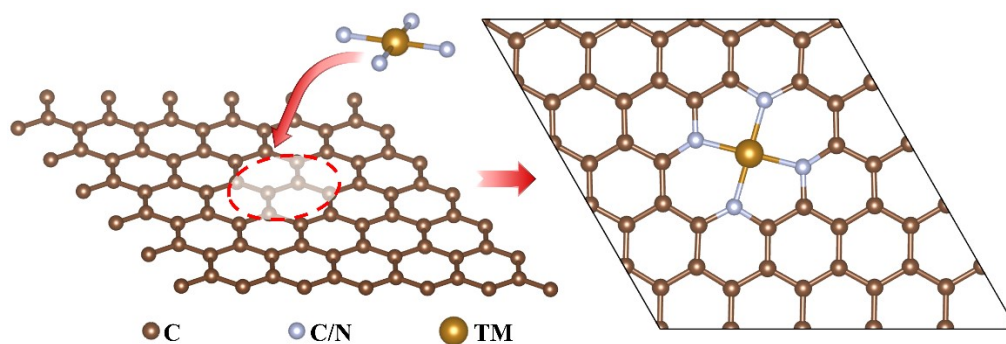
2 Supplementary Figures
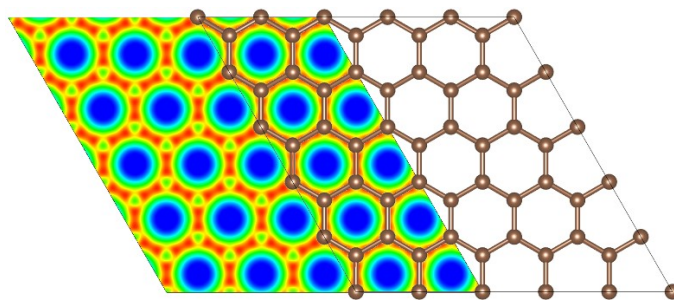
**Figure S1.** The charge density diagram of graphene.

Figure S2. The carbon network of (a) graphene and (b) T-graphene.


Figure S3. The schematic diagram of the formation process of TM-Gra. Brown and gold balls represent carbon (C) and 3d TM respectively. Gray balls represent carbon (C) in TMC_4-Gra and nitrogen (N) in TMN_4-Gra configurations. Red dashed box represents the atoms replaced on the T-graphene support.
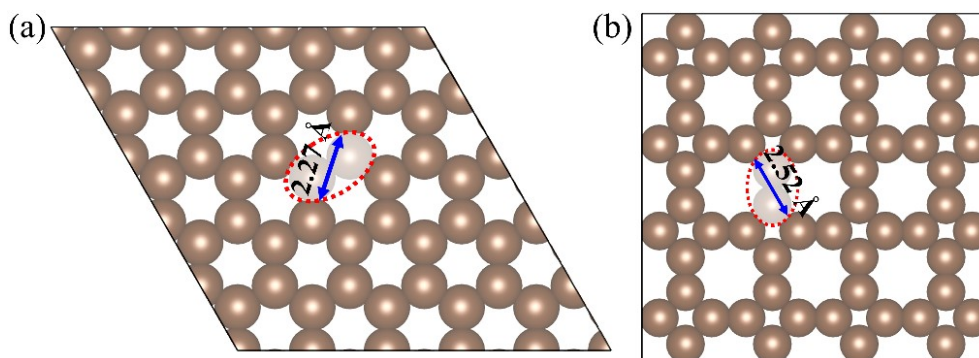
Figure S4. The illustration of dual-vacancy pore size in (a) graphene and (b) T-graphene.
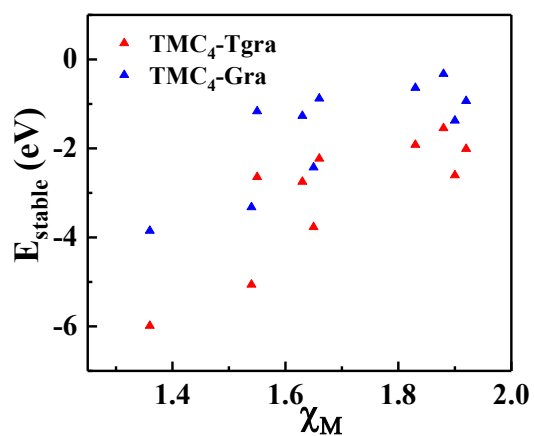
Figure S5. The stable energy (E_{stable}) of TMC_4 located on T-graphene and graphene materials *versus* the electronegativity of metal.
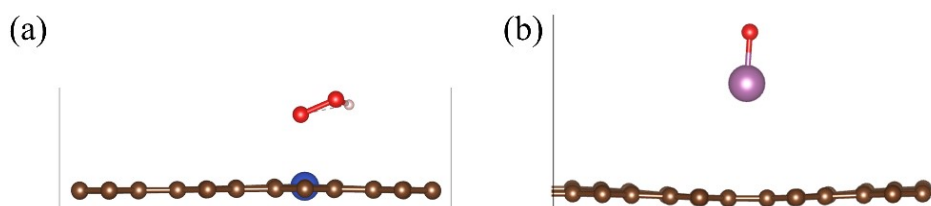
Figure S6. The optimized configuration of (a) CuC_4-Tgra and (b) ScC_4-Tgra adsorbing oxygen intermediates.
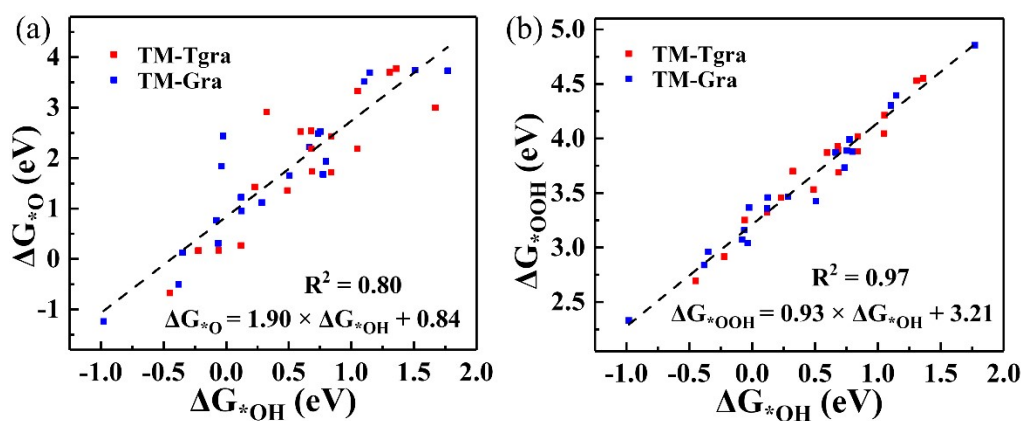
Figure S7. The relationship of (a) ΔG_{*O} *versus* ΔG_{*OH} and (b) ΔG_{*OOH} *versus* ΔG_{*OH}.
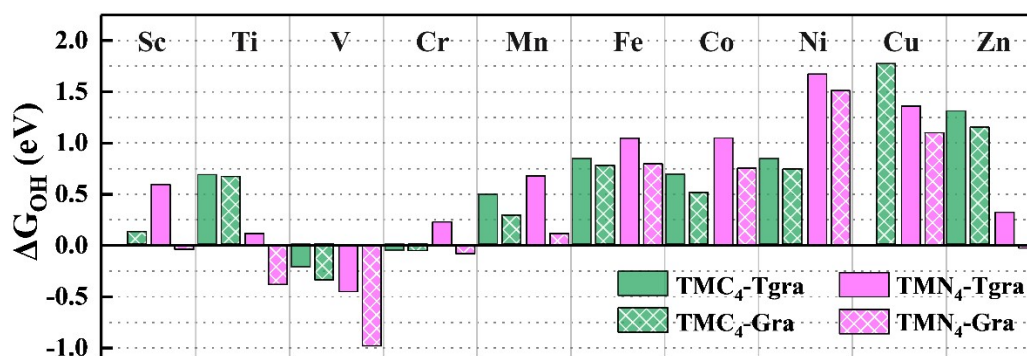
Figure S8. *OH adsorption energy (ΔG_{*OH}) of all TM-Tgra and TM-Gra.
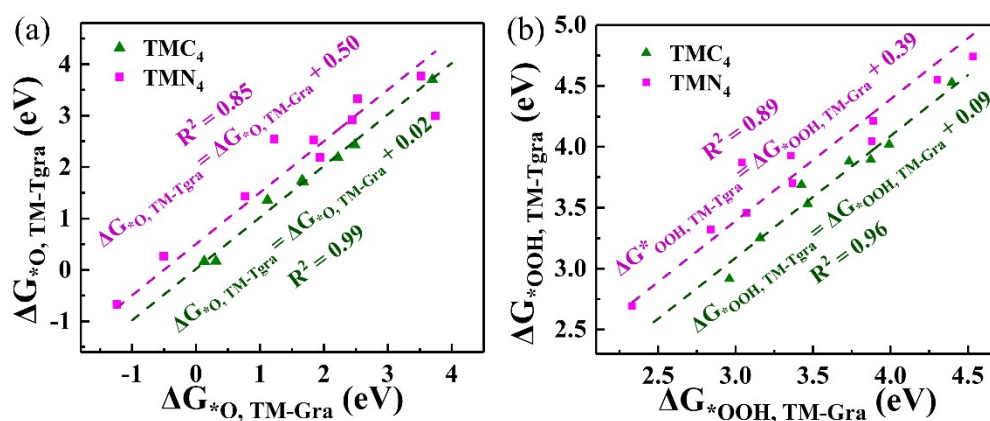
Figure S9. The relationship of (a) ΔG_{*O} of TM-Tgra *versus* ΔG_{*O} of TM-Gra and (b) ΔG_{*OOH} of TM-Tgra *versus* ΔG_{*OOH} of TM-Gra.
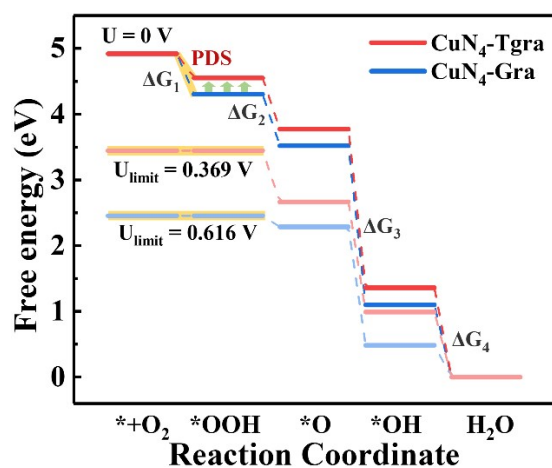
Figure S10. The free energy diagram of CuN_4 with weak binging strength with intermediates.
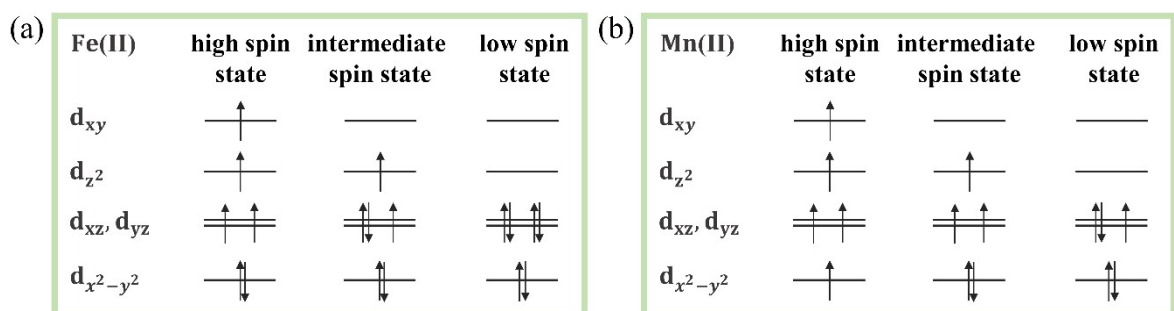
Figure S11. The d-orbital electronic arrangement of (a) Fe(II) and (b) Mn(II) with high, intermediate and low spin states.
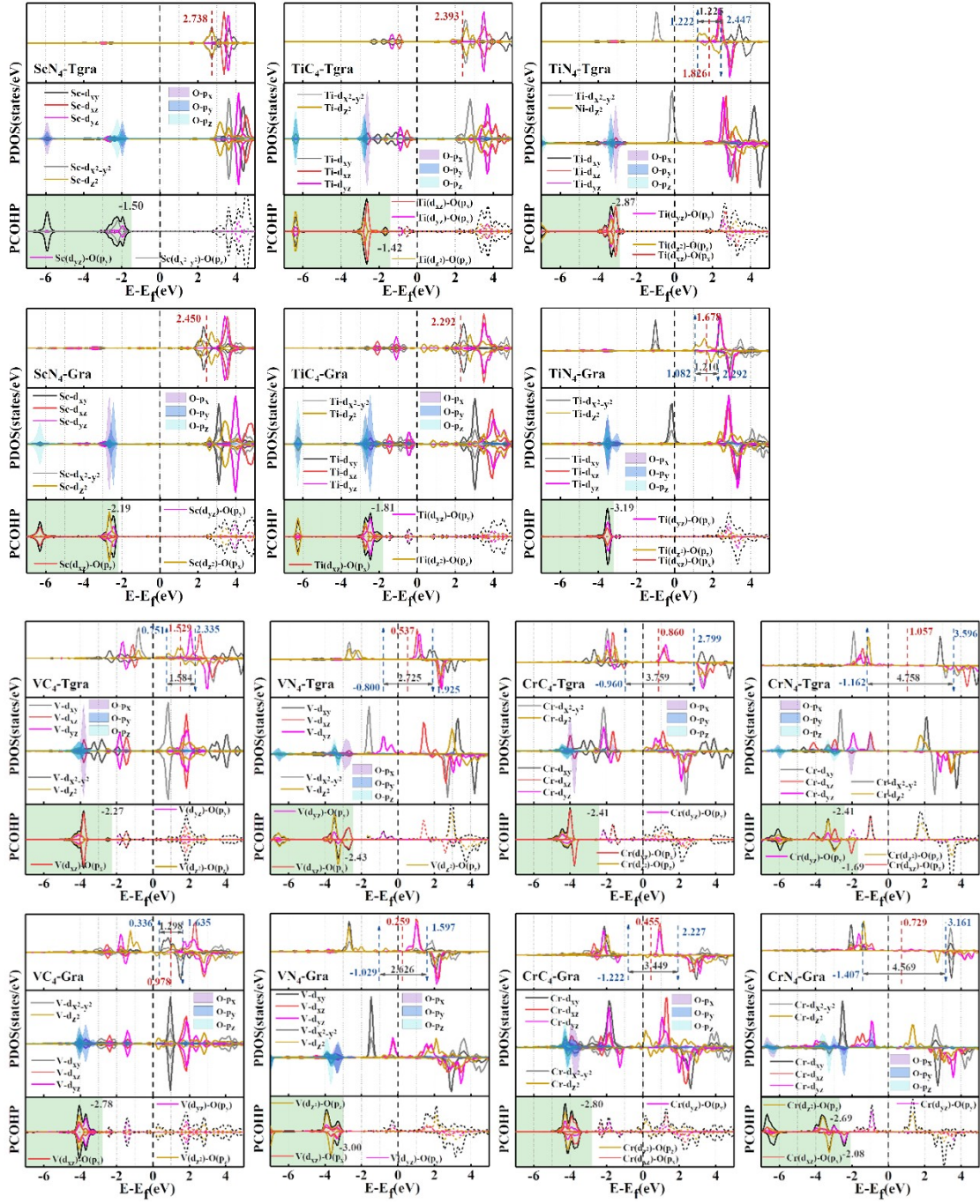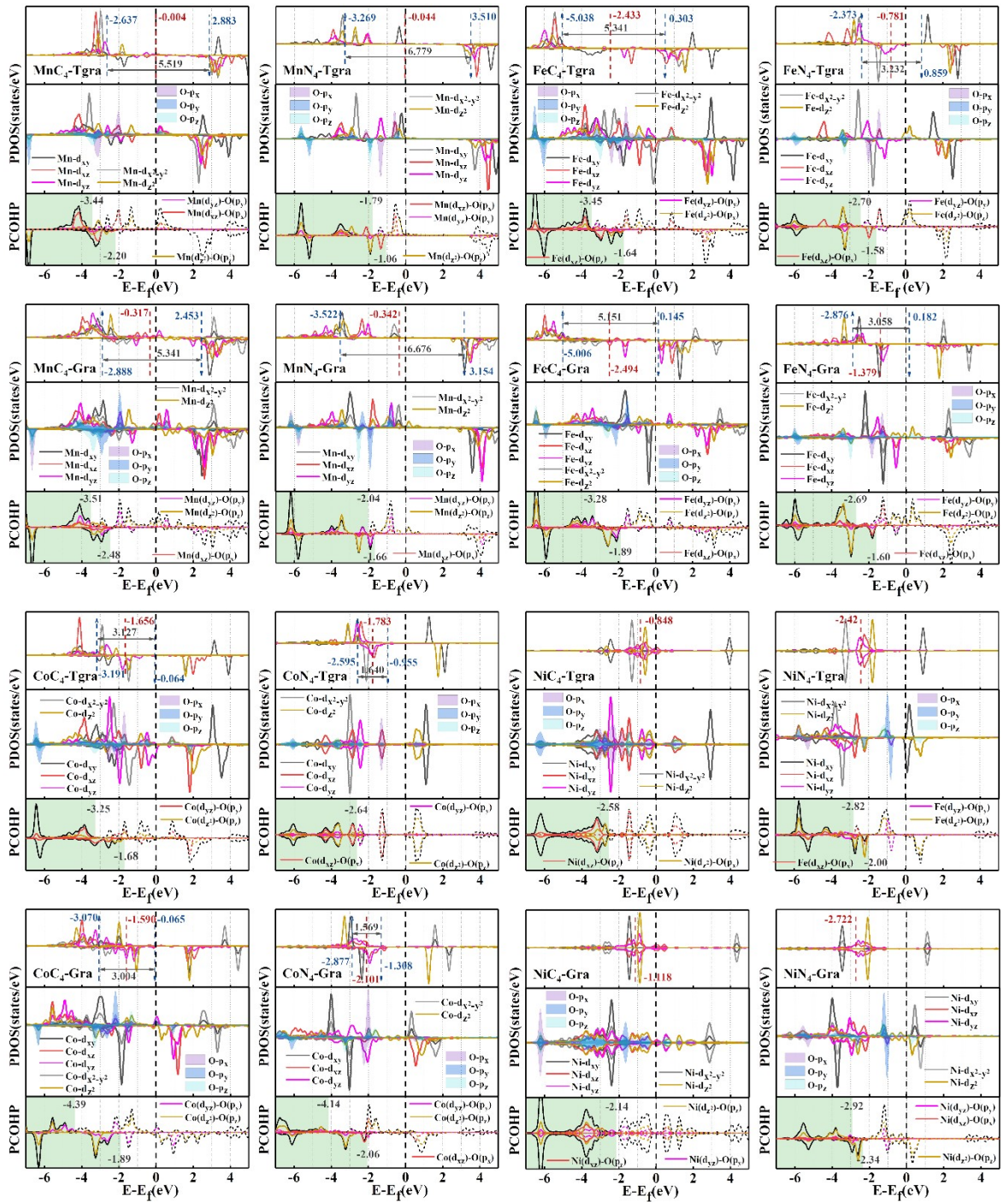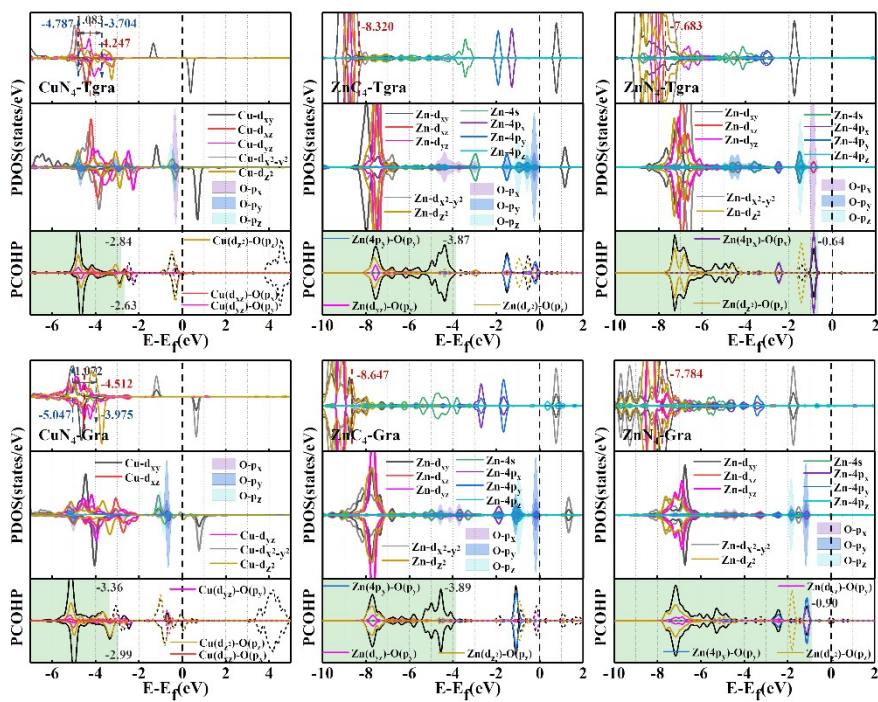
Figure S12. PDOS and PCOHP before and after adsorbing *OH on TM-Tgra and TM-Gra.
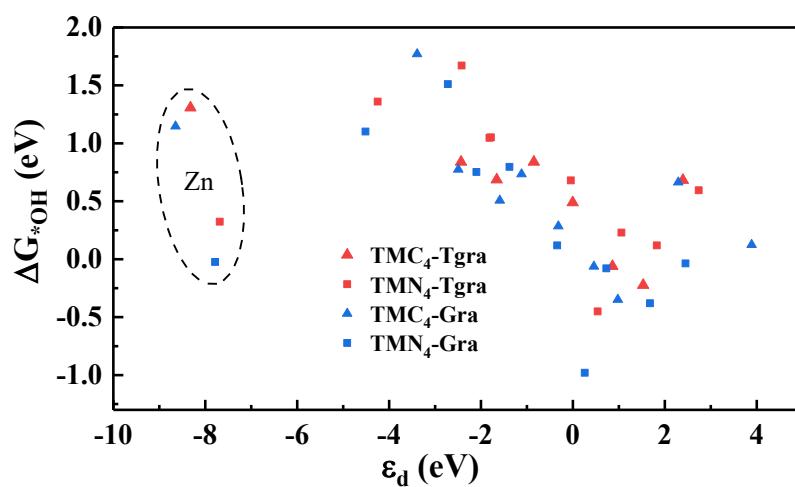
Figure S13. The relationship of ΔG*OH *versus* d-band center (εd).
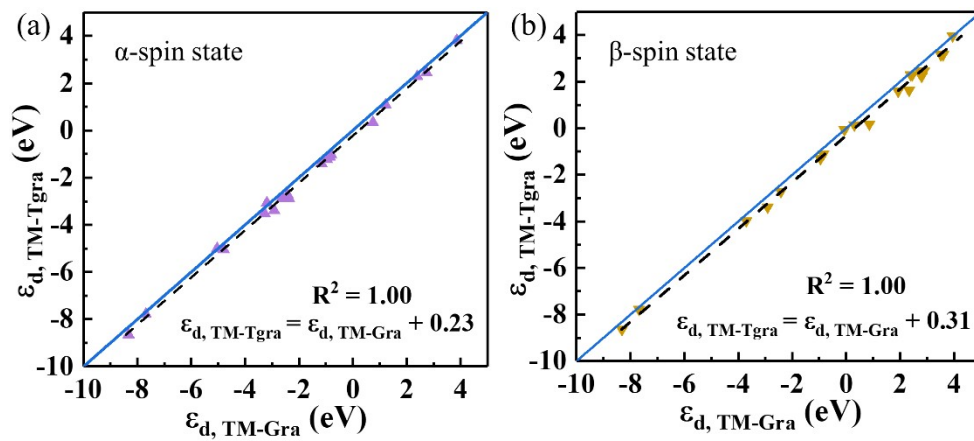
Figure S14. The relationship between (a) α-spin state and (b) β-spin state d-band centers of TM-Tgra and that of TM-Gra.

3 Supplementary Tables

Table S1 The values of U−J parameters for DFT/PBE+U calculations.[22]

Sc	Ti	V	Cr	Mn	Fe	Co	Ni	Cu	Zn
2.11	2.58	2.72	2.79	3.06	3.29	3.42	3.40	3.87	4.12

Table S2 The values used for zero-point energy corrections (eV).

Species	Adsorbed on clean slab
*O	0.070
*OH	0.330
*OOH	0.430

Table S3 Energy values for H_2O, O_2 and H_2.

	Pressure (bar)	E_{DFT} (eV)	ZPE (eV)	G (eV)
$O_2(g)$	1	−	−	−9.900
$H_2(g)$	1	−6.773	−0.045	−6.818
$H_2O(l)$	0.035	−14.228	−0.000	−14.228

Table S4 The properties of 3d-transition metals.

TM	E_{TM} (eV)	χ_M[23]	r_M (Å)[23]
Sc	–6.647	1.36	1.59
Ti	–8.458	1.54	1.48
V	–9.688	1.63	1.44
Cr	–10.017	1.66	1.30
Mn	–9.374	1.55	1.29
Fe	–8.600	1.83	1.24
Co	–7.461	1.88	1.18
Ni	–5.939	1.91	1.17
Cu	–4.319	1.90	1.22
Zn	–1.520	1.65	1.20

Table S5 The stability energy (eV) of all TM-Tgra and TM-Gra configurations.

TM	TMC_4-Tgra	TMN_4-Tgra	TMC_4-Gra	TMN_4-Gra
Sc	–5.986	–6.104	–3.851	–5.030
Ti	–5.062	–3.306	–3.322	–2.594
V	–2.750	–1.174	–1.270	–0.355
Cr	–2.231	–1.198	–0.881	–0.752
Mn	–2.643	–1.175	–1.165	–0.595
Fe	–1.921	–0.078	–0.639	–0.137
Co	–1.547	0.209	–0.326	–0.037
Ni	–2.012	–0.246	–0.934	–0.610
Cu	–2.604	–0.013	–1.377	0.012
Zn	–3.771	–2.233	–2.430	–1.897

Table S6 Adsorption free energies of *OH, *O and *OOH (eV) and ORR onset potential (U_{onset}) (V) on TM-Tgra and TM-Gra. And reaction barriers ($\Delta G_1 \sim \Delta G_4$) (eV) of ORR elementary reactions at 1.23 V on TM-Tgra and TM-Gra.

	*OH	*O	*OOH	U_{onset}	ΔG_1	ΔG_2	ΔG_3	ΔG_4
ScC$_4$-Tgra	–	–	–	–	–	–	–	–
TiC$_4$-Tgra	0.682	2.186	3.896	0.682	0.206	–0.48	–0.274	0.548
VC$_4$-Tgra	–0.223	0.166	2.916	–0.223	–0.774	–1.52	0.841	1.453
CrC$_4$-Tgra	–0.060	0.170	3.253	–0.060	–0.437	–1.853	1.000	1.290
MnC$_4$-Tgra	0.489	1.357	3.532	0.489	–0.158	–0.945	0.362	0.741
FeC$_4$-Tgra	0.839	1.716	4.020	0.839	0.330	–1.074	0.353	0.391
CoC$_4$-Tgra	0.686	1.737	3.689	0.686	–0.001	–0.722	0.179	0.544
NiC$_4$-Tgra	0.840	2.432	3.881	0.840	0.191	–0.219	–0.362	0.390
CuC$_4$-Tgra	–	–	–	–	–	–	–	–
ZnC$_4$-Tgra	1.308	3.698	4.529	0.391	0.839	0.399	–1.160	–0.078
ScN$_4$-Tgra	0.595	2.523	3.872	0.595	0.182	–0.119	–0.698	0.635
TiN$_4$-Tgra	0.119	0.269	3.322	0.119	–0.368	–1.823	1.080	1.111
VN$_4$-Tgra	–0.450	–0.675	2.694	–0.450	–0.996	–2.139	1.455	1.680
CrN$_4$-Tgra	0.229	1.431	3.458	0.229	–0.232	–0.797	0.028	1.001
MnN$_4$-Tgra	0.679	2.539	3.928	0.679	0.238	–0.159	–0.630	0.551
FeN$_4$-Tgra	1.048	2.186	4.046	0.874	0.356	–0.630	0.092	0.182
CoN$_4$-Tgra	1.051	3.331	4.214	0.706	0.524	0.347	–1.050	0.179
NiN$_4$-Tgra	1.672	2.995	4.740	0.180	1.050	–0.515	–0.093	–0.442
CuN$_4$-Tgra	1.360	3.773	4.551	0.369	0.861	0.452	–1.183	–0.130
ZnN$_4$-Tgra	0.323	2.915	3.701	0.323	0.011	0.444	–1.362	0.907
ScC$_4$-Gra	0.124	0.951	3.460	0.124	–0.230	–1.279	0.403	1.106
TiC$_4$-Gra	0.664	2.219	3.872	0.664	0.182	–0.423	–0.325	0.566
VC$_4$-Gra	–0.349	0.129	2.960	–0.349	–0.730	–1.601	0.752	1.579
CrC$_4$-Gra	–0.063	0.310	3.158	–0.063	–0.532	–1.618	0.857	1.293
MnC$_4$-Gra	0.284	1.118	3.465	0.284	–0.225	–1.117	0.396	0.946
FeC$_4$-Gra	0.774	1.677	3.991	0.774	0.301	–1.084	0.327	0.456
CoC$_4$-Gra	0.507	1.657	3.425	0.507	–0.265	–0.538	0.08	0.723

NiC$_4$-Gra	0.734	2.484	3.732	0.734	0.042	−0.018	−0.520	0.496
CuC$_4$-Gra	1.770	3.730	4.855	0.065	1.165	0.105	−0.730	−0.540
ZnC$_4$-Gra	1.146	3.697	4.396	0.524	0.706	0.531	−1.321	0.084
ScN$_4$-Gra	−0.037	1.841	3.041	−0.037	−0.649	0.030	−0.648	1.267
TiN$_4$-Gra	−0.381	−0.506	2.839	−0.381	−0.851	−2.115	1.355	1.611
VN$_4$-Gra	−0.980	−1.236	2.331	−0.980	−1.359	−2.337	1.486	2.210
CrN$_4$-Gra	−0.079	0.768	3.072	−0.079	−0.618	−1.074	0.383	1.309
MnN$_4$-Gra	0.119	1.224	3.358	0.119	−0.332	−0.904	0.125	1.111
FeN$_4$-Gra	0.797	1.933	3.880	0.797	0.190	−0.717	0.094	0.433
CoN$_4$-Gra	0.753	2.524	3.888	0.753	0.198	−0.134	−0.541	0.477
NiN$_4$-Gra	1.511	3.743	4.533	0.387	0.843	0.440	−1.002	−0.281
CuN$_4$-Gra	1.102	3.519	4.304	0.616	0.614	0.445	−1.187	0.128
ZnN$_4$-Gra	−0.024	2.439	3.367	−0.024	−0.323	0.302	−1.233	1.254

Table S7 The α-spin ($\varepsilon_{d, \alpha}$), β-spin state ($\varepsilon_{d, \beta}$), and total electronic state (ε_d) d-band center of TM-Tgra and TM-Gra.

	$\varepsilon_{d, \alpha}$ (eV)	$\varepsilon_{d, \beta}$ (eV)	ε_d (eV)
ScC$_4$-Tgra	3.861	3.948	3.905
TiC$_4$-Tgra	2.393	2.393	2.393
VC$_4$-Tgra	0.751	2.335	1.529
CrC$_4$-Tgra	−0.960	2.799	0.860
MnC$_4$-Tgra	−2.637	2.883	−0.004
FeC$_4$-Tgra	−5.038	0.303	−2.433
CoC$_4$-Tgra	−3.191	−0.064	−1.656
NiC$_4$-Tgra	−0.849	−0.848	−0.848
CuC$_4$-Tgra	−2.914	−2.913	−2.913
ZnC$_4$-Tgra	−8.322	−8.319	−8.320
ScN$_4$-Tgra	2.737	2.739	2.738
TiN$_4$-Tgra	1.222	2.447	1.826
VN$_4$-Tgra	−0.800	1.925	0.537
CrN$_4$-Tgra	−1.162	3.596	1.057
MnN$_4$-Tgra	−3.269	3.510	−0.044
FeN$_4$-Tgra	−2.373	0.859	−0.781
CoN$_4$-Tgra	−2.595	−0.955	−1.783
NiN$_4$-Tgra	−2.422	−2.421	−2.421
CuN$_4$-Tgra	−4.787	−3.704	−4.247
ZnN$_4$-Tgra	−7.684	−7.682	−7.683
ScC$_4$-Gra	3.815	3.965	3.889
TiC$_4$-Gra	2.288	2.295	2.292
VC$_4$-Gra	0.336	1.635	0.978
CrC$_4$-Gra	−1.222	2.227	0.455
MnC$_4$-Gra	−2.888	2.453	−0.317
FeC$_4$-Gra	−5.006	0.145	−2.494
CoC$_4$-Gra	−3.070	−0.065	−1.590
NiC$_4$-Gra	−1.118	−1.117	−1.118
CuC$_4$-Gra	−3.390	−3.387	−3.389
ZnC$_4$-Gra	−8.649	−8.644	−8.647

ScN$_4$-Gra	2.449	2.450	2.450
TiN$_4$-Gra	1.082	2.292	1.678
VN$_4$-Gra	−1.029	1.597	0.259
CrN$_4$-Gra	−1.407	3.161	0.729
MnN$_4$-Gra	−3.522	3.154	−0.342
FeN$_4$-Gra	−2.876	0.182	−1.379
CoN$_4$-Gra	−2.877	−1.308	−2.101
NiN$_4$-Gra	−2.723	−2.722	−2.722
CuN$_4$-Gra	−5.047	−3.975	−4.512
ZnN$_4$-Gra	−7.785	−7.783	−7.784

Reference

1. Kresse, G.; Furthmüller, J., Efficiency of ab-initio total energy calculations for metals and semiconductors using a plane-wave basis set. *Computational Materials Science* **1996,** *6*, 15-50.

2. Kresse, G.; Furthmüller, J., Efficient iterative schemes for ab initio total-energy calculations using a plane-wave basis set. *PHYSICAL REVIEW B* **1996,** *54* (16), 11169-11185.

3. Perdew, J. P.; Burke, K.; Ernzerhof, M., Generalized Gradient Approximation Made Simple. **1996,** *77* (18), 3865-3868.

4. Xia, D.; Yang, X.; Xie, L.; Wei, Y.; Jiang, W.; Dou, M.; Li, X.; Li, J.; Gan, L.; Kang, F., Direct Growth of Carbon Nanotubes Doped with Single Atomic Fe–N4 Active Sites and Neighboring Graphitic Nitrogen for Efficient and Stable Oxygen Reduction Electrocatalysis. *Advanced Functional Materials* **2019,** *29* (49), 1906174.

5. Chen, Y.; Gao, R.; Ji, S.; Li, H.; Tang, K.; Jiang, P.; Hu, H.; Zhang, Z.; Hao, H.; Qu, Q.; Liang, X.; Chen, W.; Dong, J.; Wang, D.; Li, Y., Atomic-Level Modulation of Electronic Density at Cobalt Single-Atom Sites Derived from Metal-Organic Frameworks: Enhanced Oxygen Reduction Performance. *Angew Chem Int Ed Engl* **2021,** *60* (6), 3212-3221.

6. Hu, X.; Chen, S.; Chen, L.; Tian, Y.; Yao, S.; Lu, Z.; Zhang, X.; Zhou, Z., What is the Real Origin of the Activity of Fe-N-C Electrocatalysts in the O(2) Reduction Reaction? Critical Roles of Coordinating Pyrrolic N and Axially Adsorbing Species. *J Am Chem Soc* **2022,** *144* (39), 18144-18152.

7. Kresse, G.; Joubert, D., From ultrasoft pseudopotentials to the projector augmented-wave method. *PHYSICAL REVIEW B* **1999,** *59* (3), 1758-1775.

8. Dudarev, S. L.; Botton, G. A.; Savrasov, S. Y.; Humphreys, C. J.; Sutton, A. P., Electron-energy-loss spectra and the structural stability of nickel oxide: An LSDA+U study. *PHYSICAL REVIEW B* **1998,** *57* (3), 1505-1509.

9. Duan, Z.; Henkelman, G., Surface Charge and Electrostatic Spin Crossover Effects in CoN4 Electrocatalysts. *ACS Catalysis* **2020,** *10* (20), 12148-12155.

10. Yin, S. H.; Yang, J.; Han, Y.; Li, G.; Wan, L. Y.; Chen, Y. H.; Chen, C.; Qu, X. M.; Jiang, Y. X.; Sun, S. G., Construction of Highly Active Metal-Containing Nanoparticles and FeCo-N(4) Composite Sites for the Acidic Oxygen Reduction Reaction. *Angew Chem Int Ed Engl* **2020,** *59* (49), 21976-21979.

11. Yao, X.; Zhu, Y.; Xia, T.; Han, Z.; Du, C.; Yang, L.; Tian, J.; Ma, X.; Hou, J.; Cao, C., Tuning Carbon Defect in Copper Single-Atom Catalysts for Efficient Oxygen Reduction. *Small* **2023,** *19* (28), e2301075.

12. Cheng, X.; Yang, J.; Yan, W.; Han, Y.; Qu, X.; Yin, S.; Chen, C.; Ji, R.;

Li, Y.; Li, G.; Li, G.; Jiang, Y.; Sun, S., Nano-geometric deformation and synergistic Co nanoparticles—Co-N4 composite sites for proton exchange membrane fuel cells. *Energy & Environmental Science* **2021,** *14* (11), 5958-5967.

13. Grimme, S.; Ehrlich, S.; Goerigk, L., Effect of the damping function in dispersion corrected density functional theory. *J Comput Chem* **2011,** *32* (7), 1456-65.

14. Grimme, S.; Antony, J.; Ehrlich, S.; Krieg, H., A consistent and accurate ab initio parametrization of density functional dispersion correction (DFT-D) for the 94 elements H-Pu. *J Chem Phys* **2010,** *132* (15), 154104.

15. Mathew, K.; Sundararaman, R.; Letchworth-Weaver, K.; Arias, T. A.; Hennig, R. G., Implicit solvation model for density-functional study of nanocrystal surfaces and reaction pathways. *J Chem Phys* **2014,** *140* (8), 084106.

16. Maintz, S.; Deringer, V. L.; Tchougreeff, A. L.; Dronskowski, R., LOBSTER: A tool to extract chemical bonding from plane-wave based DFT. *J Comput Chem* **2016,** *37* (11), 1030-5.

17. Deringer, V. L.; Tchougreeff, A. L.; Dronskowski, R., Crystal orbital Hamilton population (COHP) analysis as projected from plane-wave basis sets. *J Phys Chem A* **2011,** *115* (21), 5461-6.

18. Wang, V.; Xu, N.; Liu, J.-C.; Tang, G.; Geng, W.-T., VASPKIT: A user-friendly interface facilitating high-throughput computing and analysis using VASP code. *Computer Physics Communications* **2021,** *267*, 108033.

19. Nørskov, J. K.; Rossmeisl, J.; Logadottir, A.; Lindqvist, L.; Kitchin, J. R.; Bligaard, T.; Jo´nsson, H., Origin of the Overpotential for Oxygen Reduction at a Fuel-Cell Cathode. *J. Phys. Chem. B* **2004,** *108*, 17886-17892.

20. Nørskov, J. K.; Bligaard, T.; Logadottir, A.; Bahn, S.; Hansen, L. B.; Bollinger, M.; Bengaard, H.; Hammer, B.; Sljivancanin, Z.; Mavrikakis, M.; Xu, Y.; Dahl, S.; Jacobsen, C. J. H., Universality in Heterogeneous Catalysis. *Journal of Catalysis* **2002,** *209* (2), 275-278.

21. Sun, Y.; Sun, S.; Yang, H.; Xi, S.; Gracia, J.; Xu, Z. J., Spin-Related Electron Transfer and Orbital Interactions in Oxygen Electrocatalysis. *Adv Mater* **2020,** *32* (39), e2003297.

22. Xu, H.; Cheng, D.; Cao, D.; Zeng, X. C., A universal principle for a rational design of single-atom electrocatalysts. *Nature Catalysis* **2018,** *1* (5), 339-348.

23. Haynes, W. M.; Lide, D. R.; Bruno, T. J., CRC Handbook of Chemistry and Physics. **2016**.